# Oligothiophene Interlayer Effect on Photocurrent Generation for Hybrid $TiO_2$/P3HT Solar Cells

**Cite as:**
**Planells, M., Abate, A., Snaith, H. J., & Robertson, N. (2014). Oligothiophene Interlayer Effect on Photocurrent Generation for Hybrid $TiO_2$ /P3HT Solar Cells. *ACS Applied Materials & Interfaces*, *6*(19), 17226-17235.**

**Manuscript received: 31/07/2014; Accepted: 18/09/2014; Article published: 26/09/2014**

# Oligothiophene Interlayer Effect on Photocurrent Generation for hybrid $TiO_2$/P3HT solar cells**

Miquel Planells,[1] Antonio Abate,[2] Henry J. Snaith[2,*] and Neil Robertson[1,*]

[1]EaStCHEM, School of Chemistry, Joseph Black Building, University of Edinburgh, West Mains Road, Edinburgh, EH9 3FJ, UK.

[2]Department of Physics, University of Oxford, Oxford OX1 3PU, UK.

[*]Corresponding author; H.J.S.: h.snaith1@physics.ox.ac.uk; N.R. neil.robertson@ed.ac.uk

[**]We thank the Engineering and Physical Sciences Research Council (EPSRC) APEX project for financial support.

**Graphical abstract:**

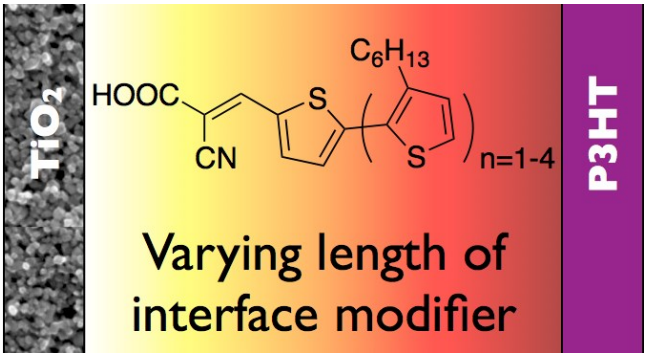

## ABSTRACT

A series of conjugated 3-hexylthiophene derivatives with a cyanoacrylic acid group has been prepared with conjugation length from one up to five thiophene units (**1T** – **5T**). The UV-Vis spectra, photoluminescence spectra, electrochemical data and DFT calculations show lowering of LUMO energies and red-shift of absorption into the visible as the thiophene chain length increases. $TiO_2$/P3HT solar cells were prepared with prior functionalization of the $TiO_2$ surface by **1T** – **5T** and studies include cells using undoped P3HT and using P3HT doped with H-TFSI. Without H-TFSI doping, photocurrent generation occurs from both the oligothiophene and P3HT. Doping the P3HT with H-TFSI quenches photocurrent generation from excitation of P3HT, but enables very effective charge extraction upon excitation of the oligothiophene. In this case, photocurrent generation increases with the light harvesting ability of **1T** – **5T** leading to a highest efficiency of 2.32% using **5T**. Overall, we have shown that P3HT can act in either charge generation or in charge collection, but does not effectively perform both functions simultaneously, and this illustrates a central challenge in the further development of $TiO_2$/P3HT solar cells.

## KEYWORDS

Solar cells / oligothiophenes / P3HT / $TiO_2$ / Dye-sensitized solar cells / organic semiconductors

## 1. INTRODUCTION

In the last decade, impressive progress has been made in solar energy, both in experimental research and market activity.[1-2] In particular, photovoltaic cells made by solution processable materials are attracting great interest as an alternative to the established silicon technologies.[3] Though a number of different device concepts have been prepared by processing both organic and inorganic materials from solution,[3] the photoactive layer is always based upon an interface between donor and acceptor semiconductors. One of the key challenges that restrict the choice of donor-acceptor combinations is the ability to achieve simultaneously an intimate contact, to guarantee an efficient charge separation at the interface, and a phase segregation to promote a percolation path for charge carrier transport to the electrodes. In fully organic devices for example, using conjugated polymers such as poly(3-hexylthiophene) (P3HT) as donor and organic small molecules such as fullerene derivatives as acceptor, the high chemical affinity of the two organic components facilitates the formation of a suitable interface, which results in efficient charge separation.[4-6] However, the same chemical affinity makes control and stabilization of the phase separation difficult, which is critical to generate percolation pathways for the charge extraction. Therefore, fully organic devices suffer from relatively low charge mobility and thermal instability of the phase segregation.[7] A potential solution to overcome these deficiencies is to combine organic and inorganic semiconductors.[8] As an example of such inorganic-organic hybrid solar cells, a transparent semiconductor such as $TiO_2$ acts as inorganic acceptor for the charges generated in the P3HT.[9-10] This device architecture is rooted in the well known dye-sensitized solar cells (DSSCs) technology, with the difference that the P3HT is acting at the same time as light absorber, instead of the dye anchored on the $TiO_2$, and hole transporter, instead of the redox electrolyte.[11] The main advantage of this approach is the possibility to prepare a mesoporous $TiO_2$ electrode, which works as scaffold for the organic component and allows control and stabilization of the phase segregation.[11] In recent work, P3HT has been used as the hole conductor along with an additional light absorber in solid-state DSSCs, with power conversion efficiencies over 3%.[10, 12] However, for these systems, almost all the photocurrent originates from light absorbed in the dye layer, and is not delivered from the P3HT. This literature indicates that electron transfer from photo-excited P3HT into $TiO_2$ does not occur very effectively. In this context, one of the key issues is the inherent incompatibility between the hydrophilic surface of the metal oxide and

the hydrophobic nature of the conjugated polymer, which limits the intimate contact between the organic donor and the inorganic acceptor.[13] Several reports showed that the quality of this interface is crucial to achieve efficient charge separation in P3HT/$TiO_2$ hybrid systems.[14-15] We note here that the quality of the P3HT/$TiO_2$ interface is completely decoupled from the issue of the $TiO_2$ pore infiltration, which has been raised in previous studies to explain $TiO_2$/P3HT device performances.[12, 16] Indeed, Canesi and co-workers demonstrated that, regardless of the pore filling fraction, the orientation and the packing of P3HT chains in contact with the $TiO_2$ surface are crucial to control the electronic coupling between the excited state energy levels in the polymer and the conduction band states in the oxide.[17] The same authors modified the $TiO_2$ surface with a molecular layer that drives local ordering of the polymer in contact with the surface, which enabled power conversion efficiency (PCE) above 1%. In another work, similar efficiency was reported by Grancini and co-workers, who observed efficient electron transfer from the photo-excited polymer to the $TiO_2$, functionalizing the metal oxide surface with fullerene derivatives.[7] In a different approach, the P3HT can be functionalized with carboxylic acid groups to directly anchoring the polymer to the $TiO_2$ and thus create a more intimate contact at $TiO_2$/P3HT interface.[16] However, despite the number of reports the effective operation of a functionalized P3HT/$TiO_2$ photoactive layer is quite poor.[13, 15, 18] The low device performances have been attributed to the presence of multiple anchoring groups on the same polymeric chain, which lowers the crystallinity of the polymer in contact with the $TiO_2$ and thus the possibility to achieve efficient charge separation.[17]

In this work, we report the synthesis and the characterization (electrochemical, optical and computational) for a series of conjugated oligo-3-hexylthiophenes (oligothiophene) derivatives, with a number of thiophene units from 1 to 5 (Fig. 1). All the molecules are functionalized with a terminal cyanoacrylic acid group that allows anchoring the oligothiophenes on $TiO_2$ surface. We use those oligothiophene functionalized $TiO_2$ to prepare $TiO_2$/P3HT solar cells and study the effect of the thiophene length on the device performance.

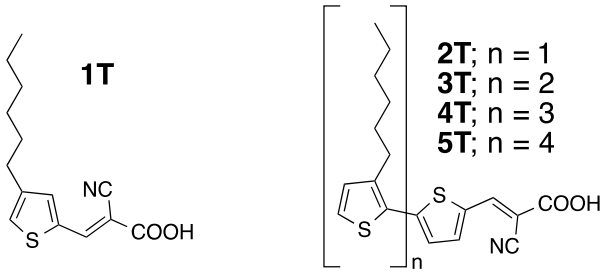


**Figure 1**. Molecular structures of the oligothiophene derivatives used in this study.

## 2. EXPERIMENTAL SECTION

### 2.1 Synthetic procedure

**Materials**. All reagents were purchased from either Sigma-Aldrich or Alfa-Aesar and were used as received without further purification, except for 5-bromo-2-thiophenecarboxaldehyde, which was purified by silica plug in $CH_2Cl_2$ and *N*-Bromosuccinimide (NBS), which was recrystallized from water.

**Synthesis of 3-hexylthiophene-5-carbaldehyde (1)**. 3-hexylthiophene (1 g, 5.9 mmol) was placed in a Schlenk tube with 15 mL of dry THF. The mixture was cooled down to –78 ºC, stirred under $N_2$ and n-butyllithium 2.5 M in hexane (2.6 mL, 6.5 mmol) was added dropwise. Afterwards, the reaction was warmed to 0 ºC and stirred for 1 h. at 0 ºC. Then, the mixture was cooled down again to –78 ºC and DMF (550 μL, 7.1 mmol) was added dropwise. Finally, the reaction was warmed to room temp. and stirred for 3 h. The mixture was poured into a 100 mL 1% HCl aqueous solution and extracted with $Et_2O$ (2 x 50 mL). The combined organic phases were joined together, washed with brine and dried over $Na_2SO_4$. After removing the solvent, the crude was purified by column chromatography ($SiO_2$, Hexanes up to Hexanes / EtOAc 20:1) to afford a mixture of isomers (85% 5-substituted / 15% 2-substituted) as colourless oil (1.06 g, 91% yield). $^1$H NMR (500 MHz, $CDCl_3$) $\delta_H$: 9.87 (s, 1H); 7.60 (s, 1H); 7.36 (s, 1H); 2.64 (t, J = 7.7, 2H); 1.63 (m, 2H); 1.31 (m, 6H); 0.89 (t, J = 6.8, 3H). $^{13}$C NMR (125 MHz, $CDCl_3$) $\delta_C$: 183.2; 145.0; 143.8; 137.3; 130.6; 31.8; 30.6; 30.3; 29.0; 22.8; 14.3. MS EI (m/z): $[M]^+$ calcd for $C_{11}H_{16}OS$: 196.09164; found: 196.091333. Anal. calcd for $C_{11}H_{16}OS$: C, 67.30; H, 8.22; found: C, 67.38; H, 8.14.

**Synthesis of (*E*)-2-cyano-3-(3-hexylthiophen-5-yl)acrylic acid (1T)**. **1** (700 mg, 3.5 mmol) and cyanoacetic acid (190 mg, 2.25 mmol) were placed in a Schlenk flask with 7 mL of EtOH. The mixture was stirred under $N_2$ and piperidine (750 μL, 17.5 mmol) was added. The reaction was heated up to 75 ºC for 3 h. Then, the mixture was poured into a 120 mL of aqueous HCl 1M and the yellow precipitate collected by filtration. Pure product was obtained by washing the cake with $H_2O$, drying and then washing with few mL of cold hexane, giving the pure product as yellow solid (680 mg, 74% yield). $^1$H NMR (500 MHz, $CDCl_3$) $\delta_H$: 13.73 (br s, 1H); 8.44 (s, 1H); 7.86 (s, 1H); 7.81 (s, 1H); 2.60 (t, J = 7.6, 2H); 1.57 (m, 2H); 1.28 (m, 6H); 0.86 (t, J = 14.1, 3H). $^{13}$C NMR (125 MHz, $CDCl_3$) $\delta_C$: 163.5; 146.9; 144.1; 144.1; 140.2; 135.3;

131.8; 116.2; 98.5; 30.9; 29.7; 29.1; 28.2; 22.0; 13.9. MS EI (m/z): $[M]^+$ calcd for $C_{14}H_{17}NO_2S$: 263.09745; found: 263.09777. Anal. calcd for $C_{20}H_{15}N$: C, 63.85; H, 6.51; N, 5.32; found: C, 63.68; H, 6.43; N, 5.22.

**Synthesis of tributyl(3-hexylthiophen-2-yl) (2)**. Mg turnings (530 mg, 22 mmol) were placed in a Schlenk flask with 10 mL of dry THF. The mixture was heated to 75 ºC under $N_2$ and stirred for 3 h. The reaction was cooled down and then transferred via cannula under $N_2$ to a solution of 2-bromo-3-hexylthiophene (5 g, 20 mmol) in 10 mL of dry THF. The resulting mixture was cooled down to –78 ºC and tributyltinchloride (6 mL, 22 mmol) was added dropwise. Then, the reaction was stirred overnight at room temp. under inert atmosphere. The crude was then poured into 200 mL of $H_2O$ and extracted with 200 mL of hexane. The organic phase was dried over $Na_2SO_4$ and solvent removed, giving a pure product as yellowish oil (9.1 g, 99% yield) which was used without further purification. $^1$H NMR (500 MHz, $CDCl_3$) $\delta_H$: 7.54 (d, J = 4.6, 1H); 7.11 (d, J = 4.7, 1H); 2.61 (t, J = 8.0, 2H); 1.57 (m, 8H); 1.33 (m, 18H); 1.13 (m, 6H); 0.91 (m, 16H). $^{13}$C NMR (125 MHz, $CDCl_3$) MS EI (m/z): $[M]^+$ calcd for $C_{22}H_{42}SSn$: 458.20237; found: 458.202735. Anal. calcd for $C_{22}H_{42}SSn$: C, 57.78; H, 9.26; found: C, 57.62; H, 9.18.

**Synthesis of 3'-hexyl-[2,2'-bithiophene]-5-carbaldehyde (3)**. Tri(*o*-tolyl)phosphine (286 mg, 0.94 mmol) and tris(dibenzylideneacetone)dipalladium (430 mg, 0.47 mmol) were placed in a Schlenk flask and dried under high vacuum for 30 minutes. Then, a solution of 5-bromo-2-thiophenecarboxaldehyde (3 g, 15.7 mmol) and **2** (7.2 g, 15.7 mmol) in dry and degassed toluene (63 mL) was transferred via cannula under Ar. The resulting solution was degassed again by pump-freeze technique and stirred at 90 ºC overnight under $N_2$. Then, 70 mL of aqueous KF 1M was added and stirred for 1 h. The organic fraction was collected, dried over $Na_2SO_4$ and solvent removed. The crude was purified by column chromatography ($SiO_2$, Hexanes / 5% EtOAc) to afford the product as yellow oil (3.01 g, 69% yield). $^1$H NMR (500 MHz, $CDCl_3$) $\delta_H$: 9.89 (s, 1H); 7.71 (d, J = 4.0, 1H); 7.28 (d, J = 5.2, 1H); 7.22 (d, J = 3.9, 1H); 6.98 (d, J = 5.2, 1H); 2.81 (t, J = 7.9, 2H); 1.65 (m, 2H); 1.38 (m, 2H); 1.31 (m, 4H); 0.88 (t, J = 7.1, 3H). $^{13}$C NMR (125 MHz, $CDCl_3$) $\delta_C$: 182.9; 146.9; 142.6; 142.3; 137.0; 130.9; 129.8; 129.8; 126.4; 126.0; 31.9; 30.6; 29.8; 29.4; 22.8; 14.3. MS EI (m/z): $[M]^+$ calcd for $C_{15}H_{18}OS_2$: 278.07936; found: 278.079133. Anal. Calcd for $C_{15}H_{18}OS_2$: C, 64.71; H, 6.52; Found: C, 64.89; H, 6.54.

**Synthesis of (*E*)-2-cyano-3-(3'-hexyl-[2,2'-bithiophen]-5-yl)acrylic acid (2T)**. **3** (200 mg, 0.72 mmol) and cyanoacetic acid (92 mg, 1.08 mmol) were placed in a Schlenk flask with 1.5 mL of EtOH. The mixture was stirred under $N_2$ and piperidine (350 μL, 3.6 mmol) was added. The reaction was heated up to 75 ºC for 3 h. Then, the mixture was poured into a 100 mL of aqueous HCl 1M and the red precipitate was collected by filtration. Pure product was obtained by washing the cake with $H_2O$, giving a red solid (89 mg, 35% yield). $^1$H NMR (500 MHz, $CDCl_3$) $\delta_H$: 8.33 (s, 1H); 7.81 (d, J = 4.1, 1H); 7.32 (d, J = 5.2, 1H); 7.27 (d, J = 4.4, 1H); 6.99 (d, J = 5.2, 1H); 2.85 (t, J = 7.9, 2H); 1.67 (m, 2H); 1.41 (m, 2H); 1.31 (m, 4H); 0.89 (t, J = 6.9, 3H). $^{13}$C NMR (125 MHz, $CDCl_3$) $\delta_C$: 167.4; 148.6; 147.8; 143.0; 139.1; 134.8; 131.1; 129.6; 126.8; 126.7; 115.8; 96.6; 31.8; 30.6; 30.0; 29.4; 22.8; 14.3. MS EI (m/z): $[M]^+$ calcd for $C_{18}H_{19}NO_2S_2$: 345.08517; found: 345.08563. Anal. calcd for $C_{18}H_{19}NO_2S_2$: C, 62.58; H, 5.54; N, 4.05; found: C, 62.47; H, 5.53; N, 3.97.

**Synthesis of 5'-bromo-3'-hexyl-[2,2'-bithiophene]-5-carbaldehyde (4)**. **3** (3 g, 10.7 mmol) was placed in a round bottom flask with 33 mL of DMF and cooled down to 0 ºC. NBS (2.28 g, 12.84 mmol) was added in small portions and the reaction was stirred overnight at room temp. Then, the mixture was poured into 200 mL of $H_2O$ and extracted with 200 mL of $Et_2O$. The organic phase was washed with brine, dried over $Na_2SO_4$ and the solvent removed. The crude was purified by column chromatography ($SiO_2$, Hexanes / 5% EtOAc) to afford the product as yellow oil (2.38 g, 62% yield). $^1$H NMR (500 MHz, $CDCl_3$) $\delta_H$: 9.89 (s, 1H); 7.69 (d, J = 3.9, 1H); 7.15 (d, J = 3.9, 1H); 6.41 (s, 1H); 2.75 (t, J = 7.8; 2H); 1.62 (m, 2H); 1.37 (m, 2H); 1.30 (m, 4H); 0.87 (t, J = 7.0, 3H). $^{13}$C NMR (125 MHz, $CDCl_3$) $\delta_C$: 182.9; 145.2; 142.9; 142.8; 136.9; 133.5; 131.2; 126.7; 113.2; 31.8; 20.5; 29.7; 22.8; 22.7; 14.3. MS EI (m/z): $[M]^+$ calcd for $C_{15}H_{17}BrOS_2$: 355.98987; found: 355.990508. Anal. Calcd for $C_{15}H_{17}BrOS_2$: C, 50.42; H, 4.80; Found: C, 50.39; H, 4.91.

**Synthesis of 3',3''-dihexyl-[2,2':5',2''-terthiophene]-5-carbaldehyde (5)**. Tri(*o*-tolyl)phosphine (121 mg, 0.4 mmol) and tris(dibenzylideneacetone)dipalladium (183 mg, 0.2 mmol) were placed in a Schlenk flask and dried under high vacuum for 30 minutes. Then, a solution of **4** (2.38 g, 6.7 mmol) and **2** (3.56 g, 3.6 mmol) in dry and degassed toluene (25 mL) was transferred via cannula under Ar. The resulting solution was degassed again by pump-freeze technique and stirred at 90 ºC overnight under $N_2$. Then, 25 mL of aqueous KF 1M was added and stirred for 1 h. The organic fraction was collected, dried over $Na_2SO_4$ and solvent removed. The crude was

purified by column chromatography ($SiO_2$, Hexanes / 5% EtOAc) to afford the product as yellow oil (2.01 g, 71% yield). $^1$H NMR (500 MHz, $CDCl_3$) $\delta_H$: 9.89 (s, 1H); 7.71 (d, J = 4.0, 1H); 7.23 (d, J = 4.0, 1H); 7.20 (d, J = 5.2, 1H); 6.98 (s, 1H); 6.94 (d, J = 5.2, 1H); 2.82 (t, J = 7.6, 2H); 2.78 (t, J = 7.8, 2H); 1.69 (m, 2H); 1.65 (m, 2H); 1.40 (m, 4H); 1.32 (m, 8H); 0.89 (m, 3H); 0.87 (m, 3H). $^{13}$C NMR (125 MHz, $CDCl_3$) $\delta_C$: 182.8; 146.5; 142.7; 142.3; 140.6; 137.1; 136.8; 130.5; 130.0; 129.4; 129.3; 126.1; 124.5; 31.9 (x2); 30.8; 30.5; 30.0; 29.6; 29.4 (x2); 22.8; 14.3 (x2). MS EI (m/z): $[M]^+$ calcd for $C_{25}H_{32}OS_3$: 444.16098; found: 444.161262. Anal. Calcd for $C_{25}H_{32}OS_3$: C, 67.52; H, 7.25; Found: C, 67.39; H, 7.13.

**Synthesis of (*E*)-2-cyano-3-(3',3''-dihexyl-[2,2':5',2''-terthiophen]-5-yl)acrylic acid (3T)**. **5** (250 mg, 0.56 mmol) and cyanoacetic acid (71 mg, 0.84 mmol) were placed in a Schlenk flask with 2.5 mL of EtOH. The mixture was stirred under $N_2$ and piperidine (275 μL, 2.8 mmol) was added. The reaction was heated up to 75 ºC for 3 h. Then, the mixture was poured into a 100 mL of aqueous HCl 1M and the formed red precipitate was collected by filtration. Pure product was obtained by washing the cake with $H_2O$, drying, stirring in $EtO_2$, and removal of the solvent, giving a deep-red solid (100 mg, 35% yield). $^1$H NMR (500 MHz, $CDCl_3$) $\delta_H$: 8.32 (s, 1H); 7.81 (d, J = 4.2, 1H); 7.27 (d, J = 4.2 1H); 7.21 (d, J = 5.3, 1H); 7.00 (s, 1H); 6.95 (d, J = 5.3, 1H); 2.85 (t, J = 7.8, 2H); 2.79 (t, J = 7.8, 2H); 1.71 (m, 2H); 1.64 (m, 2H); 1.45 (m, 2H); 1.39 (m, 2H); 1.32 (m, 8H); 0.90 (m, 3H); 0.89 (m, 3H). $^{13}$C NMR (125 MHz, $CDCl_3$) $\delta_C$: 167.2; 148.1; 147.5; 143.5; 140.8; 139.1; 137.6; 134.6; 130.5; 129.9; 129.5; 129.2; 126.4; 124.7; 116.0; 96.4; 31.9 (x2); 30.7; 30.4; 30.2; 29.6; 29.4 (x2); 22.8 (x2) 14.3 (x2). MS EI (m/z): $[M]^+$ calcd for $C_{28}H_{33}NO_2S_3$: 511.16679; found: 511.166823. Anal. Calcd for $C_{28}H_{33}NO_2S_3$: C, 65.71; H, 6.50; N, 2.74; Found: C, 65.83; H, 6.57; N, 2.80.

**Synthesis of 5''-bromo-3',3''-dihexyl-[2,2':5',2''-terthiophene]-5-carbaldehyde (6)**. **5** (2 g, 4.5 mmol) was placed in a round bottom flask with 14 mL of DMF and cooled down to 0 ºC. NBS (800 mg, 4.5 mmol) was added in small portions and the reaction was stirred overnight at room temp. Then, the mixture was poured into 200 mL of $H_2O$ and extracted with 200 mL of $Et_2O$. The organic phase was washed with brine, dried over $Na_2SO_4$ and the solvent removed. The crude was purified by column chromatography ($SiO_2$, Hexanes / 5% EtOAc) to afford the product as yellow oil (2 g, 85% yield). $^1$H NMR (500 MHz, $CDCl_3$) $\delta_H$: 9.89 (s, 1H); 7.71 (d, J = 4.0, 1H); 7.22 (d, J = 4.0, 1H); 6.91 (s, 1H); 6.90 (s, 1H); 2.80 (t, J = 7.9, 2H); 2.71 (t, J = 7.9, 2H);

1.67 (m, 2H); 1.61 (m, 2H); 1.41 (m, 2H); 1.37 (m, 2H); 1.31 (m, 8H); 0.89 (m, 6H). $^{13}$C NMR (125 MHz, $CDCl_3$) $\delta_C$: 182.8; 146.1; 142.6; 142.5; 141.1; 137.0; 135.3; 133.1; 131.5; 129.9; 129.6; 126.4; 111.3; 31.8 (x2); 30.7; 30.4; 29.9; 29.5; 29.4; 29.3; 22.8 (x2); 14.3 (x2). MS EI (m/z): $[M]^+$ calcd for $C_{25}H_{31}BrOS_3$: 522.07149; found: 522.071220. Anal. Calcd for $C_{25}H_{31}BrOS_3$: C, 57.35; H, 5.97; Found: C, 60.44; H, 6.27.

**Synthesis of 3',3'',3'''-trihexyl-[2,2':5',2'':5'',2'''-quaterthiophene]-5-carbaldehyde (7)**. Tri(*o*-tolyl)phosphine (69 mg, 0.23 mmol) and tris(dibenzylideneacetone)dipalladium (105 mg, 0.115 mmol) were placed in a Schlenk flask and dried under high vacuum for 30 minutes. Then, a solution of **6** (2 g, 3.82 mmol) and **2** (1.92 g, 4.2 mmol) in dry and degassed toluene (15 mL) was transferred via cannula under Ar. The resulting solution was degassed again by pump-freeze technique and stirred at 90 ºC overnight under $N_2$. Then, 10 mL of aqueous KF 1M was added and stirred for 1 h. The organic fraction was collected, dried over $Na_2SO_4$ and solvent removed. The crude was purified by column chromatography ($SiO_2$, Hexanes / 5% EtOAc) to afford the product as orange oil that solidifies at –20 ºC (1.66 g, 71% yield). $^1$H NMR (500 MHz, $CDCl_3$) $\delta_H$: 9.89 (s, 1H); 7.71 (d, J = 4.0, 1H); 7.24 (d, J = 4.0, 1H); 7.17 (d, J = 5.1, 1H); 7.00 (s, 1H); 6.95 (s, 1H); 6.94 (d, J = 5.1, 1H); 2.83 (t, J = 7.8, 2H); 2.78 (t, J = 7.8, 4H); 1.69 (m, 6H); 1.42 (m, 6H); 1.33 (m, 12H); 0.69 (m, 9H). $^{13}$C NMR (125 MHz, $CDCl_3$) $\delta_C$: 182.7; 146.5; 142.7; 142.3; 140.8; 140.1; 137.1; 136.5; 135.1; 130.5; 130.4; 128.8; 129.4; 129.1; 129.0; 126.0; 124.5; 31.9 (x3); 30.8; 30.6; 30.5; 30.0; 29.7; 29.5; 29.4 (x3); 22.8 (x3); 14.3 (x3). MS EI (m/z): $[M]^+$ calcd for $C_{35}H_{46}OS_4$: 610.24260; found: 610.242491. Anal. Calcd for $C_{35}H_{46}OS_4$: C, 68.80; H, 7.59; Found: C, 68.98; H, 7.43.

**Synthesis of (*E*)-2-cyano-3-(3',3'',3'''-trihexyl-[2,2':5',2'':5'',2'''-quaterthiophen]-5-yl)acrylic acid (4T)**. **7** (611 mg, 1 mmol) and cyanoacetic acid (130 mg, 1.5 mmol) were placed in a Schlenk flask with 4 mL of EtOH. The mixture was stirred under $N_2$ and piperidine (500 µL, 5 mmol) was added. The reaction was heated up to 75 ºC for 5 h. Then, the mixture was poured into a 100 mL of aqueous HCl 1M and the red-dark precipitate was centrifuged 15 minutes at 4400 r.p.m. The precipitate was dissolved in $CHCl_3$, dried over $Na_2SO_4$, giving the pure product as deep-red solid (626 mg, 92% yield). $^1$H NMR (500 MHz, $CDCl_3$) $\delta_H$: 8.30 (s, 1H); 7.80 (d, J = 4.1, 1H); 7.27 (d, J = 4.1, 1H); 7.17 (d, J = 5.2, 1H); 7.01 (s, 1H); 6.95 (s, 1H); 6.93 (d, J = 5.2, 1H); 2.86 (t, J = 7.9, 2H); 2.79 (m, 4H); 1.69 (m, 6H); 1.43 (m,

6H); 1.34 (m, 12H); 0.91 (m, 9H). $^{13}$C NMR (125 MHz, $CDCl_3$) $\delta_C$: 168.3; 148.3; 147.5; 143.7; 141.1; 140.1; 139.4; 137.4; 135.4; 134.5; 130.4 (x2); 129.7; 129.2 (x2); 129.1; 126.3; 124.1; 115.9; 96.1; 31.9 (x3); 30.8; 30.6; 30.4; 30.3; 29.8; 29.6; 29.5 (x3); 22.8 (x3); 14.3 (x3). MS EI (m/z): $[M]^+$ calcd for $C_{38}H_{47}NO_2S_4$: 677.24841; found: 677.248566. Anal. Calcd for $C_{38}H_{47}NO_2S_4$: C, 67.31; H, 6.99; N, 2.07; Found: C, 67.22; H, 7.03; N, 2.17.

**Synthesis of 5'''-bromo-3',3'',3'''-trihexyl-[2,2':5',2'':5'',2'''-quaterthiophene]-5-carbaldehyde (8)**. **7** (1 g, 1.64 mmol) was placed in a round bottom flask with 8 mL of DMF and cooled down to 0 ºC. NBS(291 mg, 1.64 mmol) was added in small portions and the reaction was stirred overnight at room temp. Then, the mixture was poured into 200 mL of $H_2O$ and extracted with 200 mL of $Et_2O$. The organic phase was washed with brine, dried over $Na_2SO_4$ and the solvent removed. The crude was purified by column chromatography ($SiO_2$, Hexanes / 5% EtOAc) to afford the product as orange oil (1.04 g, 92% yield). $^1$H NMR (500 MHz, $CDCl_3$) $\delta_H$: 9.89 (s, 1H); 7.71 (d, J = 4.0, 1H); 7.24 (d, J = 4.0, 1H); 6.99 (s, 1H); 6.89 (s, 1H); 6.88 (s, 1H); 2.82 (t, J = 7.8, 2H); 2.77 (t, J = 7.8, 2H); 2.71 (t, J = 7.8, 2H); 1.68 (m, 4H); 1.61 (m, 2H); 1.32 (m, 18H); 0.89 (m, 9H). $^{13}$C NMR (125 MHz, $CDCl_3$) $\delta_C$: 182.8; 146.3; 142.7; 142.4; 140.8; 140.6; 137.1; 136.1; 133.6; 132.9; 131.9; 130.4; 129.6; 129.4; 129.3; 126.1; 110.8; 31.8 (x3); 30.7; 30.6; 30.4; 30.0; 29.6; 29.4 (x3); 29.3; 22.8 (x3); 14.3 (x3). MS EI (m/z): $[M]^+$ calcd for $C_{35}H_{45}BrOS_4$: 688.15311; found: 688.153678. Anal. Calcd for $C_{35}H_{45}BrOS_4$: C, 60.93; H, 6.57; Found: C, 60.83; H, 6.46.

**Synthesis of 3',3'',3''',3''''-tetrahexyl-[2,2':5',2'':5'',2''':5''',2''''-quinquethiophene]-5-carbaldehyde (9)**. Tri(*o*-tolyl)phosphine (28 mg, 90 μmol) and tris(dibenzylideneacetone)dipalladium (41 mg, 45 μmol) were placed in a Schlenk flask and dried under high vacuum for 30 minutes. Then, a solution of **8** (1.04 g, 1.50 mmol) and **2** (760 mg, 1.66 mmol) in dry and degassed toluene (6 mL) was transferred via cannula under Ar. The resulting solution was degassed again by pump-freeze technique and stirred at 90 ºC overnight under $N_2$. Then, 10 mL of aqueous KF 1M was added and stirred for 1 h. The organic fraction was collected, dried over $Na_2SO_4$ and solvent removed. The crude was pre-purified by a silica plug ($CHCl_3$) and then column chromatography ($SiO_2$, Hexanes / 5% EtOAc) to afford the product as orange-red oil that solidifies at –20 ºC (833 mg, 72% yield). $^1$H NMR (500 MHz, $CDCl_3$) $\delta_H$: 9.89 (s, 1H); 7.71 (d, J = 4.0, 1H); 7.24 (d, J = 4.0, 1H); 7.17 (d, J = 5.2,

1H); 7.01 (s, 1H); 6.97 (s, 1H); 6.97 (s, 1H); 6.93 (d, J = 5.2, 1H); 2.83 (t, J = 7.9, 2H); 2.78 (m, 6H); 1.69 (m, 8H); 1.42 (m, 8H); 1.33 (m, 16H); 0.90 (m, 12H). $^{13}$C NMR (125 MHz, $CDCl_3$) $\delta_C$: 182.7; 146.4; 142.8; 142.3; 140.8; 140.2; 139.9; 137.1; 136.4; 134.7; 134.6; 130.6; 130.4; 130.3; 129.8; 129.4; 129.1; 129.0; 128.8; 126.1; 123.9; 31.9 (x4); 30.9; 30.7 (x2); 30.5; 30.0; 29.7 (x2); 29.5; 29.4 (x4); 22.8 (x4); 14.3 (x4). MS EI (m/z): $[M]^+$ calcd for $C_{45}H_{60}OS_5$: 776.32422; found: 776.324025. Anal. Calcd for $C_{45}H_{60}OS_5$: C, 69.53; H, 7.78; Found: C, 69.51; H, 7.77.

**Synthesis of (*E*)-2-cyano-3-(3',3'',3''',3''''-tetrahexyl-[2,2':5',2'':5'',2''':5''',2''''-quinquethiophen]-5-yl)acrylic acid (5T)**. **9** (200 mg, 0.26 mmol) and cyanoacetic acid (33 mg, 0.39 mmol) were placed in a Schlenk flask with 2 mL of EtOH. The mixture was stirred under $N_2$ and piperidine (130 μL, 1.30 mmol) was added. The reaction was heated up to 75 ºC for 5 h. Then, the mixture was poured into 100 mL of aqueous HCl (1M) and extracted with $Et_2O$. The crude was purified by size exclusion chromatography (Bio-beads S-X1, $CH_2Cl_2$) to afford the product as deep-red solid (118 mg, 54% yield). $^1$H NMR (500 MHz, $CDCl_3$) $\delta_H$: 8.32 (s, 1H); 7.82 (d, J = 4.4, 1H); 7.29 (d, J = 4.3, 1H); 7.17 (d, J = 5.2, 1H); 7.03 (s, 1H); 6.98 (s, 1H); 6.95 (s, 1H); 6.93 (d, J = 5.2, 1H); 2.87 (t, J = 7.8, 2H); 2.79 (m, 6H); 1.70 (m, 8H); 1.44 (m, 8H); 1.34 (m, 16H); 0.90 (m, 9H). $^{13}$C NMR (125 MHz, $CDCl_3$) $\delta_C$: 166.5; 148.0; 147.4; 143.5; 141.0; 140.2; 139.8; 139.1; 137.2; 134.9; 134.5; 134.4; 130.4; 130.2; 130.0; 129.5; 129.1; 129.0; 128.8; 128.7; 126.2; 123.7; 115.8; 95.8; 31.7 (x4); 30.7; 30.5; 30.4; 30.2; 30.1; 29.6; 29.5; 29.3; 29.2 (x4); 22.6 (x4); 14.1 (x4). MS EI (m/z): $[M]^+$ calcd for $C_{48}H_{61}NO_2S_5$: 843.33004; found: 843.330356. Anal. Calcd for $C_{48}H_{61}NO_2S_5$: C, 68.28; H, 7.28; N, 1.66; Found: C, 68.16; H, 7.19; N, 1.62.

### 2.2 Methods

*Chemical characterisation*. $^1$H and $^{13}$C NMR spectra were recorded on Bruker Advance 500 spectrometer (500 MHz for $^1$H and 125 MHz for $^{13}$C). The deuterated solvents are indicated; chemical shifts, δ, are given in ppm, referenced to TMS, standardized by the solvent residual signal ($^1$H, $^{13}$C). Coupling constants (J) are given in hertz (Hz). MS were recorded on ThermoElectron MAT 900 using electron impact (EI) ionization technique. Elemental analyses were carried out by Stephen Boyer at London Metropolitan University using a Carlo Erba CE1108 Elemental Analyser.

*Electrochemical characterisation*. All cyclic voltammetry measurements were carried out in freshly distilled $CH_2Cl_2$ using 0.3 M [TBA][$PF_6$] electrolyte in a three-

electrode system, with each solution being purged with $N_2$ prior to measurement. The working electrode was a Pt disk. The reference electrode was Ag/AgCl and the counter electrode was a Pt rod. All measurements were made at room temp. using an μAUTOLAB Type III potentiostat, driven by the electrochemical software GPES. Cyclic voltammetry (CV) measurements used scan rates of 25, 50, 100, 200 and 500 mV/s. Square wave voltammetry (SWV) experiments were carried out at a step potential of 4 mV, a square wave amplitude of 25 mV and a square wave frequency of 15 Hz, giving a scan rate of 40 mV/s. Ferrocene was used as internal standard in each measurement.

*Optical characterisation*. Solution UV-Visible absorption spectra were recorded using Jasco V-670 UV/Vis/NIR spectrophotometer controlled using the SpectraManager software. Photoluminescence (PL) spectra were recorded with Fluoromax-3 fluorimeter controlled by the ISAMain software. All samples were measured in a 1 cm cell at room temp. with dichloromethane as a solvent. Concentration of $2 \cdot 10^{-5}$ M and $5 \cdot 10^{-6}$ M were used for UV/Visible and PL, respectively.

*Computational details*. The molecular structures were optimized first in vacuum without any symmetry constrains, followed by the addition of $CH_2Cl_2$ solvation via a conductor-like polarizable continuum model (C-PCM).[19] The presence of local minimum was confirmed by the absence of imaginary frequencies. All calculations were carried out using the Gaussian 09 program[20] with the Becke three parameter hybrid exchange, Lee Yang-Parr correlation functional (B3LYP) level of theory. All atoms were described by the 6-31G(d) basis set. All structures were input and processed through the Avogadro software package.[21]

*Solar cells fabrication.* Solar cells were prepared following the procedure we previously reported.[22] All solvents used for device fabrication were reagent grade and anhydrous. FTO substrates (7 Ω/sq, Pilkington US) were etched with zinc powder and HCl (2 M aqueous solution) to give the desired electrode patterning. The substrates were cleaned with Hellmanex (2% by volume in water, Aldrich), de-ionized water, acetone, and ethanol. The last traces of organic residues were removed by 10 minutes oxygen plasma cleaning. The FTO sheets were subsequently coated with a compact layer of $TiO_2$ (about 70 nm) by aerosol spray pyrolysis deposition at 275 °C, using oxygen as the carrier gas and titanium diisopropoxide bis(acetylacetonate) as precursor. Films of 1.5 μm thick mesoporous $TiO_2$ were then deposited by screen-

printing a commercial paste (Dyesol 18NR-T). The $TiO_2$ films were slowly heated to 500 °C and allowed to sinter for 30 min in air. Once cooled, the samples were immersed into a 15 mM $TiCl_4$ aqueous solution for 45 min at 70 °C and then heated to 500 °C for another sintering step of 45 min. After cooling to 70 °C, the substrates were immersed in a 500 μM solution of oligothiophene in 1:1 v:v mixture of acetonitrile and *tert*-butyl alcohol, for 30 min. After the $TiO_2$ functionalization, the films were rinsed in acetonitrile, the P3HT was applied by spin-coating at 1000 rpm for 45 s in air from solution (30 mg/mL in chlorobenzene).[17, 23] Bis(trifluoromethanesulfonyl)imide (H-TFSI) was added in the P3HT solution prior to spinning as previously described where appropriate.[22] After drying overnight, back contacts were applied by thermal evaporation of 150 nm of silver.

*Solar cells performance characterization*.[24] For measuring the device merit parameters, simulated AM 1.5 sunlight was generated with a class AAB ABET solar simulator calibrated to give simulated AM 1.5, 100 $mWcm^{-2}$ irradiance, using an NREL-calibrated KG5 filtered silicon reference cell, with less than 1% mismatch factor; the current-voltage curves were recorded with a sourcemeter (Keithley 2400, USA). The solar cells were masked with a metal aperture defining the active area (0.12 $cm^2$) of the solar cells.

*External Quantum Efficiency (EQE).* Photovoltaic action spectra were measured (2400 Series SourceMeter, Keithley Instruments) with chopped monochromatic light incident which were biased with white light-emitting diodes (LED) at an equivalent solar irradiance of 100 $mW \cdot cm^{-2}$. The monochromatic light intensity for the incident photon-to-electron conversion efficiency was calibrated with a UV-enhanced silicon photodiode. The solar cells were masked with a metal aperture to define the active area which was typically 0.12 $cm^2$ and measured in a light-tight sample holder to minimize any edge effects.

## 3. RESULTS AND DISCUSSION

### 3.1 Synthesis

The synthetic route used to obtain the oligothiophene series is shown in Scheme 1. Synthesis of **1T** was not straightforward, since the formylation at the 5-substituted position was not fully selective. **1** was obtained as an isomeric mixture in a 15:85 ratio between 2- and 5-substituted carbaldehydes (confirmed by $^{1}$H NMR – ESI) and further separation was not possible by conventional purification techniques. However, by controlling carefully the reaction times, the 5-substituted carbaldehyde isomer reacted completely to **1T** whereas the 2-substituted isomer remained unaffected due to higher steric hindrance (confirmed by $^{1}$H NMR – ESI). This allowed us to purify the mixture by simply washing the crude with neat hexane. For **2T** to **5T**, palladium catalysed cross-coupling reactions were carried out in order to systematically increase the thiophene core chain length. In our case, we chose Stille coupling over Suzuki because higher yields were obtained. Then, selective bromination at the thiophene 5-position was attained by using NBS in dry DMF. Finally, the cyanoacrylic group was attached *via* Knoevenagel condensation for all molecules.

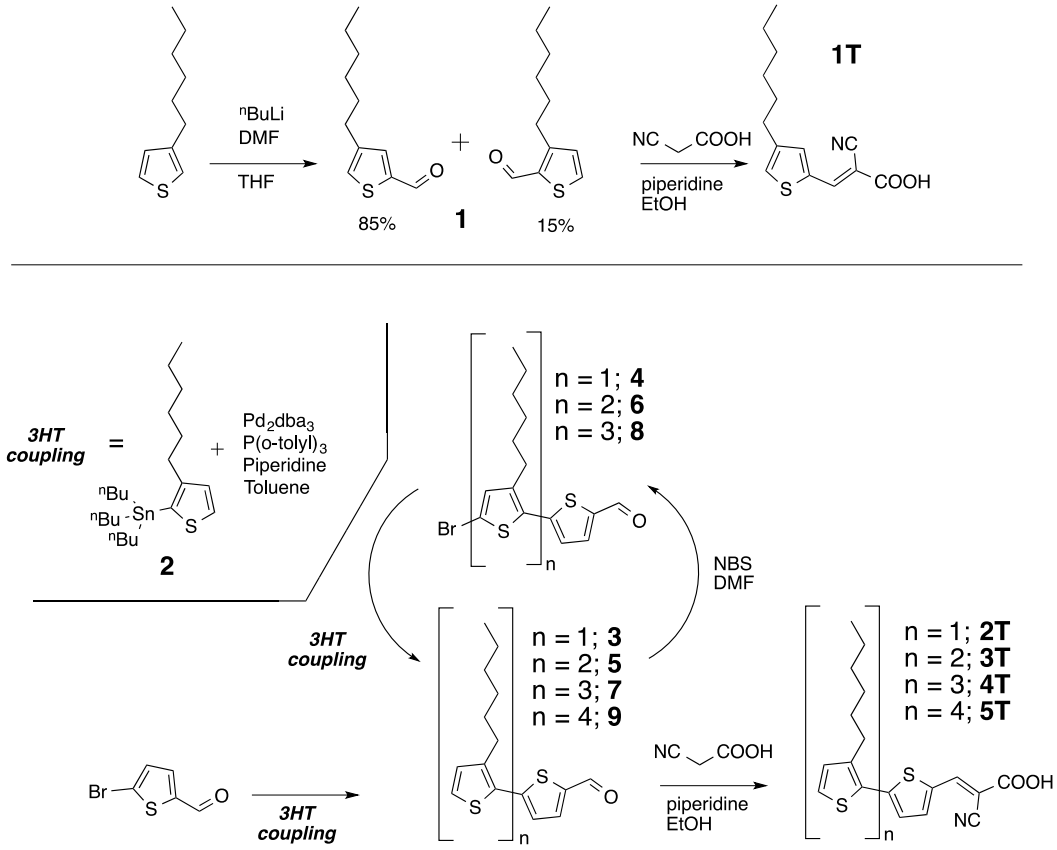


**Scheme 1**. Synthetic procedure for the synthesis of oligothiophene series.

### 3.1 Optical properties

Optical properties of our oligothiophene series were studied in dichloromethane solution. As expected, a systematic increment of the thiophene units led to red-shifted and more intense bands (Figure 2). This is due to the extra conjugation and electron delocalisation within the thiophene backbone, which reduces the molecular HOMO-LUMO gap. Therefore, **1T** showed only absorption in the UV region while visible absorption was attained after increasing the 3HT chain length, with a gradual red shift. In addition, we observed that the absorption spectral shape of **5T** was concentration dependent (ESI). Interestingly, this behaviour is not observed in any of the other oligothiophene materials reported in this study. We believe that at the working concentration range for optical studies (from $10^{-6}$ to $10^{-4}$ M), π-π stacking interactions between molecules becomes significant after the addition of the fifth 3HT unit, but not before.

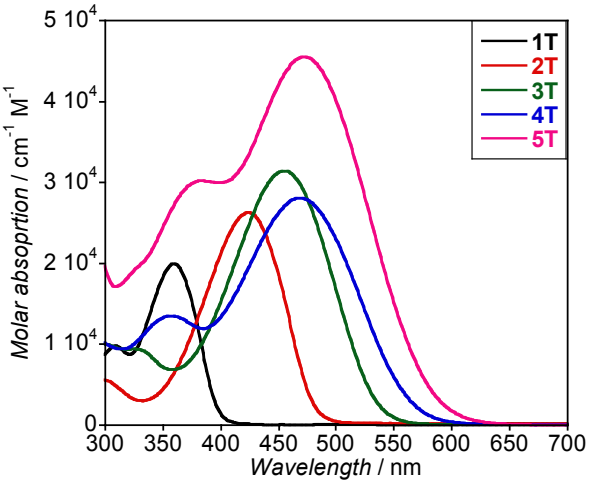


**Figure 2**. Absorbance spectra of oligothiophene molecules acquired at 5 x $10^{-5}$ M in $CH_2Cl_2$. We should note that the **5T** absorption is for its aggregated form at this concentration (ESI).

Photoluminescence (PL) was also studied in solution and is shown in Fig. 3. In this case, no PL was observed for the smaller oligothiophene molecules (**1T** and **2T**), however, it was seen for the larger derivatives, covering the visible and even the near-IR region with a very large Stokes-shift (from 4500 to 6500 $cm^{-1}$).[25] The optical gap was extracted by the absorption onset and all optical data are shown in Table 1.

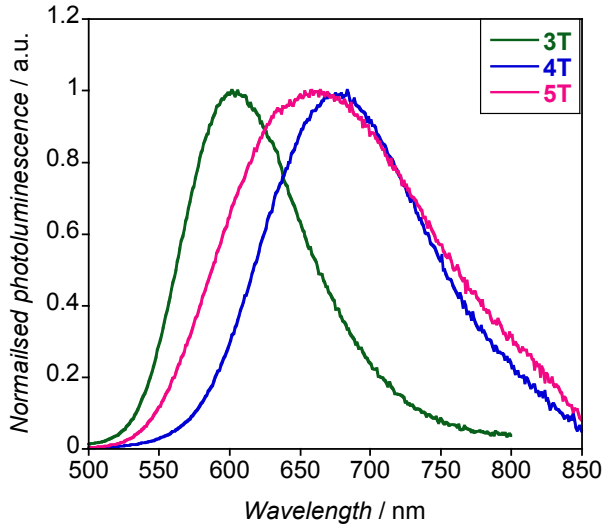


**Figure 3**. Photoluminescence (PL) spectra of emissive oligothiophene molecules acquired at $5 \cdot 10^{-6}$ M $CH_2Cl_2$ solutions and excited at $\lambda_{max}$. **1T** and **2T** did not show PL.

### 3.2 Electrochemistry

Electrochemical properties for the oligothiophene series were evaluated by cyclic (CV) and square-wave (SWV) voltammetries and referenced to ferrocene (Fig. 4 and ESI). Both oxidation and reduction processes can be observed for the whole series, except for **1T**. In this case, the oxidation potential lies beyond the solvent electrochemical window. We observe a clear trend in the oxidation potentials as we increase the thiophene core length. As expected, an increment in electron-rich substituents (*i.e.* addition of thiophene units) shifts the oxidation peaks to less positive potential and reduces the electrochemical gap between the first oxidation and first reduction potentials. Irreversible electrochemical traces were observed for **2T**, **3T** and **4T** indicating that those molecules do not generate stable cations in solution on electrochemical timescales ($10^{-1}$ – 1 s). However, those materials might work well in functional devices as the oxidised cation is regenerated by the hole transport material at much faster timescales ($10^{-10}$ – $10^{-9}$ s), which it may prevent decomposition. On the other hand, it is notable that **5T** shows reversible electrochemical behaviour, even in solution (ESI).

For the reduction processes, we can see a slight shift to less negative potentials after increasing the thiophene chain length. This shift between molecules in the series is in general much smaller than that observed for the oxidation processes, and negligible

for longer thiophene units. This is because the LUMO is localised mainly over both the cyanoacrylic moiety and its directly attached first thiophene unit, as shown later in the text by DFT calculations. Thus, the reduction processes is nearly independent of the thiophene chain length.

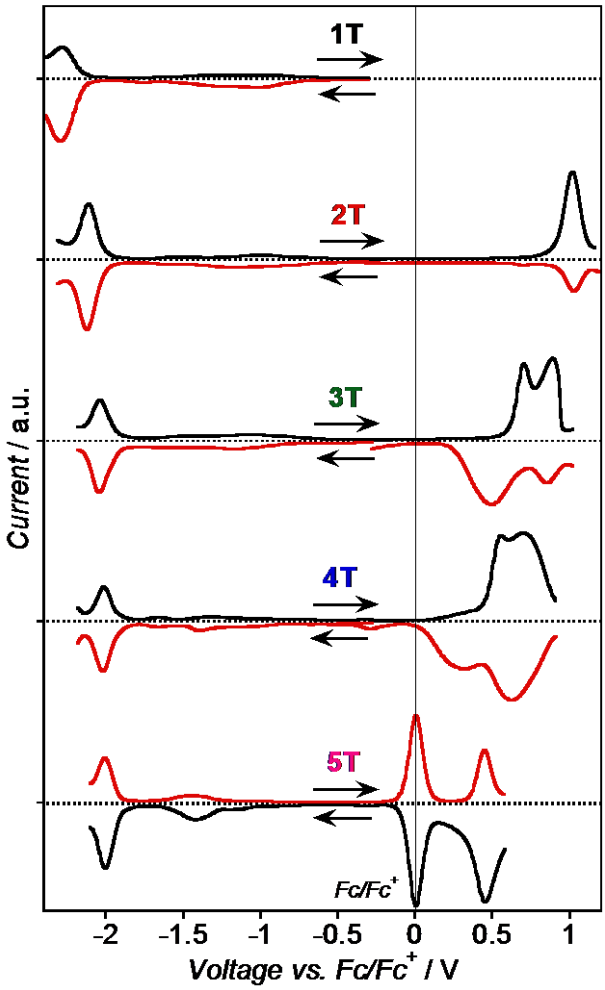


**Figure 4**. SWV of oligothiophene derivatives recorded in $CH_2Cl_2$ solution containing 0.3 M [TBA][$PF_6$] and referenced internally to ferrocene (showed in **5T** scan only). Arrows indicate the direction of scan. The small broad band located between -1.0 and -1.5 V for all samples has been attributed to the reduction of carboxylic protons.

**Table 1**. Summary of optical and electrochemical properties for the oligothiophene series acquired in $CH_2Cl_2$ solution.

| | $\lambda_{max}$ (nm) | $\varepsilon$ ($cm^{-1}$ $M^{-1}$) | $\lambda_{em}$ (nm) | $E_{gap}^{OPT}$ (eV)[a] | $E_{OX}$ (V)[b] | $E_{RED}$ (V)[b] | $E_{gap}^{CV}$ (eV)[c] | $E_{gap}^{CV} - E_{gap}^{OPT}$ (eV) |
|---|---|---|---|---|---|---|---|---|
| **1T** | 360 | 21 700 | n/o[d] | 3.10 | n/o | – 2.20 | n/a[e] | n/a |
| **2T** | 425 | 28 250 | n/o | 2.58 | + 0.92 | – 2.04 | 2.90 | 0.38 |
| **3T** | 455 | 32 000 | 600 | 2.31 | + 0.66 | – 1.95 | 2.50 | 0.30 |

| | | | | | | | | |
|---|---|---|---|---|---|---|---|---|
| **4T** | 470 | 28 000 | 675 | 2.19 | + 0.50 | – 1.94 | 2.33 | 0.25 |
| **5T** | 436-472 [f] | 45 700 | 660 | 2.12 | + 0.39 | – 1.92 | 2.25 | 0.19 |

[a]Optical gap obtained from the absorption onset. [b]Obtained from the oxidation (reduction) peak onsets. [c]Electrochemical gap = $E_{OX} - E_{RED}$. [d]Not observed. [e]Not available. [f]Optical properties are concentration dependent (ESI).

The gap obtained from electrochemical measurements follows the same trend as the optical gap, but is 0.2 to 0.4 eV larger. This is not unexpected, because the coulombic exciton binding energy is not included in the electrochemical measurement.[26] In addition, we observed that the excition binding energy was reduced by increasing the thiophene chain length, indicating greater spatial separation of the electron-hole pair, in a good agreement with the literature.[27]

### 3.3 Computational studies

Hybrid DFT calculations were performed, using Gaussian 09, B3LYP/6-31G(d) level of theory, in order to shed light on the optical and electrochemical experimental results. After applying the solvent contribution *via* C-PCM, the computed values for the HOMO and LUMO energy levels were compared to experimental values obtained from electrochemistry measurements.

In this case and due to the non-fully reversible electrochemical nature of our oligothiophene molecules, we converted the electrochemically measured potentials (V) into energy levels *versus* vacuum (eV) with the following equation: $E_{HOMO/LUMO}$ (eV *vs*. vacuum) = – 4.88 – $E_{OX/RED}$ (V *vs*. $Fc/Fc^+$).[28] As can be seen in Table 2, the computed values for $E_{LUMO}$ are accurately predicted, showing an error of ±0.1 eV. In addition, there is not much variation among samples, as the LUMO electron density is (de)localised on the cyanoacrylic moiety and its adjacent thiophene only (Fig. 5). This motif is present in the whole series and therefore we observe only a small shift in $E_{LUMO}$, in a good agreement with our electrochemical data.

On the other hand, the difference between the calculated and experimental $E_{HOMO}$ energies are much more severe. In this case, $E_{HOMO}$ was overestimated by 0.4 eV for **1T**, well matched for **2T** and underestimated by 0.2 eV for **3T**, **4T** and **5T**. However, the trend where a deeper $E_{HOMO}$ is obtained upon reducing the number of thiophene units is clear and matches with our experimental values. Moreover, the orbital

distribution is (de)localised over all thiophene units and consistent with the considerable shift of the $E_{HOMO}$ (and as consequence in the energy gap) upon increasing the thiophene chain length, as observed in both electrochemical and optical measurements (Fig. 2 and Fig. 4).

Table 2 also shows the experimental energy for the excited state (i.e. energy level from which photoinjection into $TiO_2$ would take place). These values were obtained using the optical gap rather than electrochemical gap to $E_{HOMO}$ and thus take into account the exciton binding energy.[26-27] As expected, $E_{Ex\ state}$ energy values are deeper than $E_{LUMO}$.

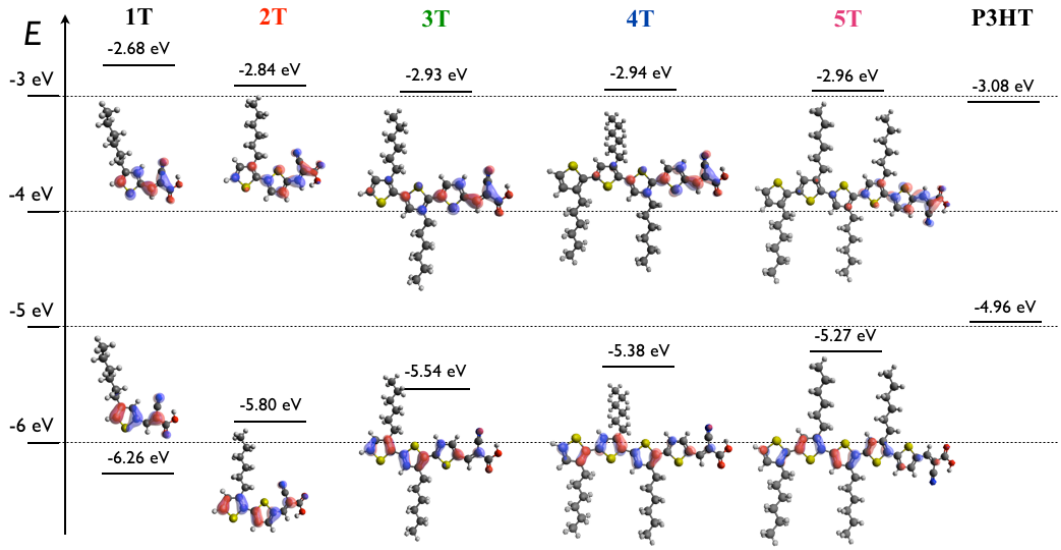


**Figure 5**. Molecular orbital distribution of HOMO (*bottom*) and LUMO (*top*) for oligothiophene series at B3LYP/6-31G(d) level of theory (isodensity = 0.04). Displayed HOMO and LUMO energy values are from experimental electrochemical measurements.

**Table 2**. Theoretical and experimental values for HOMO and LUMO energy levels in eV *vs* vacuum.

| | **DFT** (C-PCM in $CH_2Cl_2$) | | **Experimental** (in $CH_2Cl_2$) | | |
|---|---|---|---|---|---|
| | $E_{HOMO}$ | $E_{LUMO}$ | $E_{HOMO}$ [a] | $E_{LUMO}$ [a] | $E_{Ex\ state}$ [b] |
| **1T** | – 6.49 | – 2.73 | – 6.26 [c] | – 2.68 | – 3.16 |
| **2T** | – 5.80 | – 2.80 | – 5.80 | – 2.84 | – 3.22 |
| **3T** | – 5.38 | – 2.84 | – 5.54 | – 2.93 | – 3.23 |
| **4T** | – 5.17 | – 2.85 | – 5.38 | – 2.94 | – 3.19 |
| **5T** | – 4.98 | – 2.86 | – 5.27 | – 2.96 | – 3.15 |
| **P3HT** | ### | ### | – 4.96 | – 2.87 [d] | – 3.08 |

[a] $E_{HOMO(LUMO)} = -4.88 - E_{OX(RED)}$. [b] $E_{Ex\ state} = E_{HOMO} + E_{gap}$ (optical). [c] Estimated HOMO value ($E_{HOMO} = E_{LUMO} - E_{gap}$ (optical) – $E_{Exciton}$). Exciton binding energy

($E_{Exciton}$) value was obtained by extrapolation of oligothiophene series (see ESI). [d]Estimated LUMO value ($E_{LUMO} = E_{HOMO} + E_{gap}$ (optical) + $E_{Exciton}$) assuming $E_{Exciton}$ = 0.2 eV by comparison with the oligothiophene series.

### 3.4 $TiO_2$/P3HT solar cell application

After having a complete picture of the molecular optical and electrochemical properties, we prepared a set of solar cells coupling oligothiophene functionalized mesoporous $TiO_2$ with P3HT, as described in the experimental section.

**Table 3**. Device merit parameters for hybrid solar cells prepared using oligothiophene functionalized $TiO_2$ and undoped P3HT.

| | $J_{SC}$ / mA cm$^{-2}$ | PCE / % | $V_{OC}$ / V | FF |
|---|---|---|---|---|
| Neat $TiO_2$ | 0.23 | 0.04 | 0.46 | 0.39 |
| **1T** | 1.31 | 0.36 | 0.47 | 0.57 |
| **2T** | 0.53 | 0.17 | 0.60 | 0.53 |
| **3T** | 1.19 | 0.69 | 0.85 | 0.67 |
| **4T** | 1.23 | 0.79 | 0.88 | 0.72 |
| **5T** | 0.42 | 0.29 | 0.99 | 0.70 |

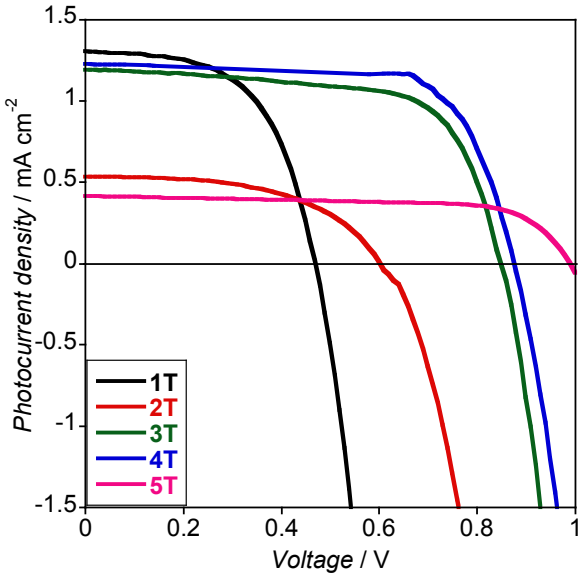


**Figure 6**. *J-V* curves for hybrid solar cells prepared with oligothiophene functionalized $TiO_2$ and undoped P3HT.

Device merit parameters and *J-V* curves are shown in Table 3 and Fig. 6, respectively. We also report the merit parameters for a device prepared with neat $TiO_2$ (no oligothiophene), which shows power conversion efficiency (PCE) significantly lower

than any of oligothiophene functionalized $TiO_2$ devices. In Table 3, we observe a strong increment in open circuit voltage ($V_{OC}$), which is proportional to the number of thiophene units present in the oligothiophene series. The $V_{OC}$ is produced by the difference between the quasi-Fermi level for electrons in the $TiO_2$ and holes in the P3HT, which is strongly affected by any dipole generated between the $TiO_2$ and the P3HT and in particular from the dipole generated by molecules directly anchored at $TiO_2$ surface. The oligothiophene molecules resulted in a dipole moment pointing away from the $TiO_2$ surface, which spreads this energy offset and thus enhances the $V_{OC}$.[29] The intensity of this dipole is proportional to the number of thiophene units (ESI), therefore a larger $V_{OC}$ is expected with the increased number of thiophene units. Otherwise, the short circuit current density ($J_{SC}$) seems not to follow any particular trend with the number of thiophene units.

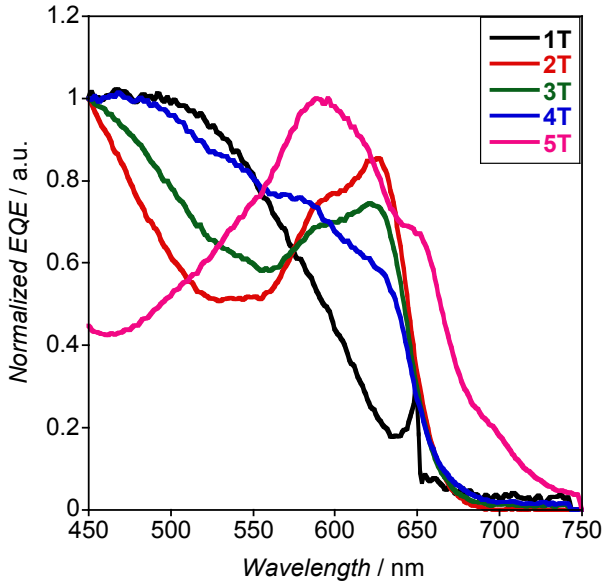


**Figure 7**. Normalized EQE for P3HT based ss-DSSC using oligothiophene series without dopant additives.

To estimate whether the photocurrent originates from light absorbed in oligothiophene or P3HT, we measured the external quantum efficiency (EQE) of the prepared devices, normalizing the spectra to the peak value between 450 and 750 nm (Fig. 7). The oligothiophene molecules absorb light up to 500 nm (depending on the number of thiophene units, see Fig. 2), while the P3HT main absorption is localized over 550 nm (ESI). In the EQE spectra in Fig. 7, we can clearly distinguish the two contributions at lower and higher wavelength, due to oligothiophene and P3HT respectively. The P3HT component becomes comparatively more pronounced than

the oligothiophene upon increasing the number of thiophene units. In particular, for **5T**, we can clearly see that the P3HT dominates the EQE spectrum, with the typical absorption due to the stacking of the polymeric chains clearly visible at 650 nm.[17]

**Table 4**. Device merit parameters for P3HT based ss-DSSC using **5T** with and without H-TFSI.

| | $J_{SC}$ / mA cm$^{-2}$ | PCE / % | $V_{OC}$ / V | FF |
|---|---|---|---|---|
| no additive | 0.42 | 0.29 | 0.99 | 0.70 |
| H-TFSI | 4.65 | 2.32 | 0.79 | 0.63 |

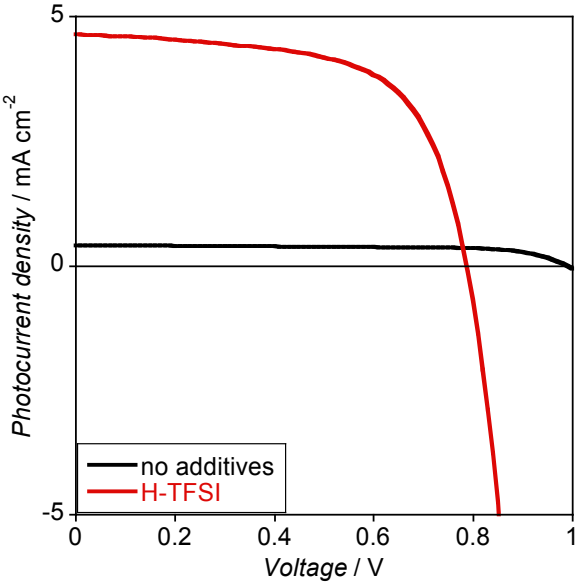


**Figure 8**. *J-V* curves for P3HT based ss-DSSC using **5T** with (*red line*) and without (*black line*) H-TFSI additive.

We prepared similar devices doping the P3HT with bis(trifluoromethanesulfonyl)imide (H-TFSI), which has been reported to improve the device performances in $TiO_2$ based solar cells.[22] Device merit parameters and *J-V* curves for devices prepared using **5T** with and without H-TFSI are shown in Table 4 and Fig. 8. We observe a 10-fold increment in $J_{SC}$ and 200 mV lower $V_{OC}$. The latter can be explained considering that the addition of H-TFSI has been described in literature to cause negative shift of $TiO_2$ conduction band, which is consistent with the observed lowering in $V_{OC}$.[22]

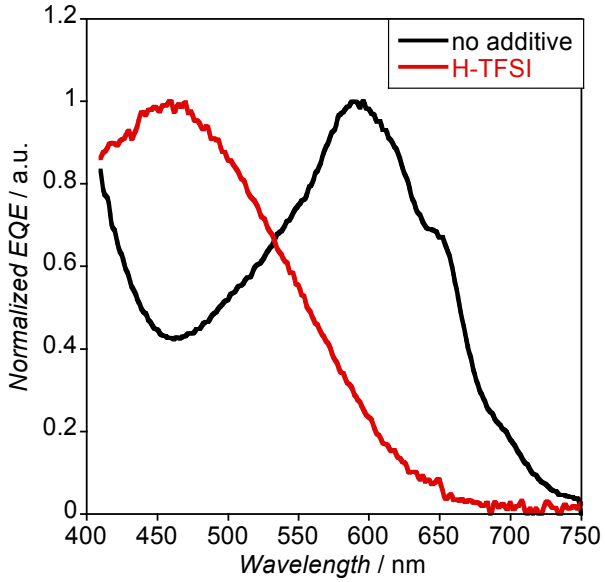


**Figure 9**. Normalized EQE for P3HT based ss-DSSC using **5T** with (*red line*) and without (*black line*) H-TFSI additive.

From the EQE spectra in Fig. 9, we see that in the H-TFSI doped device the photocurrent mainly originates from **5T** (absorption peak at 450 nm), with the P3HT contribution being comparative negligible. Doping the P3HT reduces the diffusion length of the photoexcited species (electron-hole pairs), which thus recombine before they can separate into free charges at $TiO_2$/P3HT interface, nullifying the P3HT contribution.[16]

**Table 5**. Device merit parameters for P3HT ss-DSSC using oligothiophene molecules with H-TFSI.

| | $J_{SC}$ / mA cm$^{-2}$ | PCE / % | $V_{OC}$ / V | FF |
|---|---|---|---|---|
| **1T** | 0.65 | 0.22 | 0.54 | 0.61 |
| **2T** | 0.67 | 0.23 | 0.59 | 0.57 |
| **3T** | 1.65 | 0.35 | 0.62 | 0.34 |
| **4T** | 4.41 | 1.54 | 0.69 | 0.50 |
| **5T** | 4.65 | 2.32 | 0.79 | 0.63 |

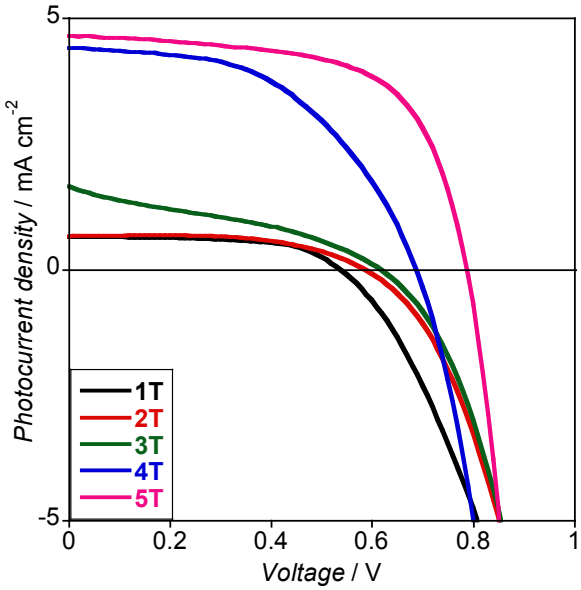


**Figure 10**. *J-V* curves for P3HT ss-DSSC using oligothiophene series with H-TFSI.

Using H-TSFI with the other oligothiophenes, we observe a clear trend not only in $V_{OC}$ as described above for devices without H-TFSI, but also for $J_{SC}$ which increases with the number of thiophene units (Table 5 and Fig. 10). Since the P3HT contribution to $J_{SC}$ is nullified with H-TFSI (Fig. 9), this increment of $J_{SC}$ can be directly correlated to the oligothiophene absorption. Indeed, increasing the number of thiophene units, the oligothiophenes absorb a larger portion of the visible spectra which allows for a larger photocurrent generation.

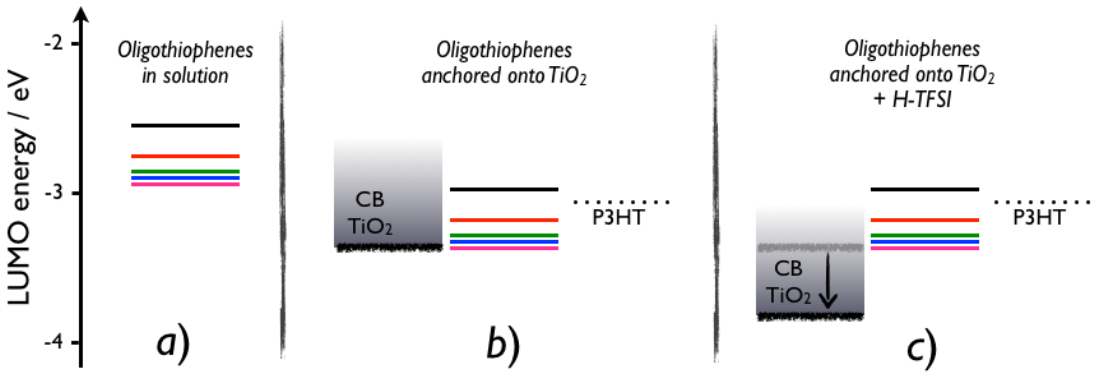


**Figure 11**. Schematic diagram of the oligothiophene LUMO energy levels: (*a*); in solution, anchored on $TiO_2$ without (*b*); and with H-TFSI doping (*c*); compared with the P3HT excited state energy level and the $TiO_2$ conduction band edge.

In Fig. 11, we propose a schematic representation of the oligothiophene energy levels relative to the P3HT, which justify the trend observed in device performances with and without the H-TFSI. In Fig. 11 - *left* we reproduced the data reported in Fig. 5, which showed that P3HT excited state level is below any of the oligothiophenes LUMO energy level. When the oligothiophenes are anchored on $TiO_2$, we need to consider that the effective LUMO levels are about 0.3 eV deeper (farther from the vacuum level) than the values measured in solution (Fig. 11 - *middle*).[23] With such a shift the P3HT excited state energy is positioned just below **1T**. This alignment explains the EQE spectrum for the **1T** device in Fig. 7, which showed negligible P3HT contribution to the photocurrent, suggesting that **1T** is acting as an energetic barrier for the electron injection. Similarly, the EQE spectrum for the **5T** device suggests that the **5T** LUMO energy should be located below or in alignment with the $TiO_2$ conduction band, since no electron injection is allowed from **5T**. In Fig. 11 - *right*, we show that doping the P3HT with H-TFSI moves the $TiO_2$ conduction toward a more negative value, which enable charge injection also for **5T** but nullifies the P3HT contribution.

## 4. CONCLUSIONS

We have reported the synthesis and characterisation of a series of conjugated 3-hexylthiophene derivatives (oligothiophenes) with a cyanoacrylic acid group, where we systematically increased the conjugation length from one up to five thiophene units. We studied their optoelectronic properties by UV-Vis, PL and electrochemical methods, showing a lowering in LUMO energies together with energy gap reduction as the thiophene chain length increases from one to five thiophene units.

We used those oligothiophenes to functionalize $TiO_2$ nanoparticles, which we employed to prepare $TiO_2$/P3HT solar cells and study the effect of thiophene length on device performances. EQE spectra showed that both oligothiophenes anchored on $TiO_2$ and P3HT can contribute to generate photocurrent. The P3HT contribution becomes comparatively more pronounced using oligothiophenes with increased number of thiophene units, but the overall device performances are significantly better with three or four thiophene units. We propose that a number of thiophene units lower or higher than three or four results in an energetic barrier for the charge extraction at the $TiO_2$/oligothiophene/P3HT interface. In particular, **1T** creates a barrier for charge collection from the P3HT, while **5T** cannot effectively inject into $TiO_2$. We also showed that doping the P3HT with H-TFSI enables a very effective charge extraction from all the oligothiophenes, but it nullifies the P3HT contribution. Hence, the use of a photoactive HTM such as P3HT, able to absorb light and transport holes, has a fundamental problem to its function. We only obtain significant photocurrent from doped devices, which mean that the device behaves as a solid state DSSC as the P3HT does not contribute to the photocurrent generation and therefore the use of a colourless HTM would be a better choice.

**SUPPORTING INFORMATION PARAGRAPH**. $^1$H-NMR spectra of **1** and **1T**. UV-Visible spectra of **5T** at different concentrations. Cyclic voltammetry at different scan rates. Exciton binding energies *vs* thiophene units. Cyclic voltammetry and UV-Visible spectrum of P3HT. Dipole moment *vs* thiophene units. "This information is available free of charge via the Internet at http://pubs.acs.org/."

## REFERENCES


(1) Dou, L.; You, J.; Hong, Z.; Xu, Z.; Li, G.; Street, R. A.; Yang, Y., 25th Anniversary Article: A Decade of Organic/Polymeric Photovoltaic Research. *Adv. Mater.* **2013**, *25*, 6642-6671.

(2) Hardin, B. E.; Snaith, H. J.; McGehee, M. D., The Renaissance of Dye-Sensitized Solar Cells. *Nat. Photonics* **2012**, *6*, 162-169.

(3) Graetzel, M.; Janssen, R. A.; Mitzi, D. B.; Sargent, E. H., Materials Interface Engineering for Solution-Processed Photovoltaics. *Nature* **2012**, *488*, 304-12.

(4) Mayer, A. C.; Scully, S. R.; Hardin, B. E.; Rowell, M. W.; McGehee, M. D., Polymer-Based Solar Cells. *Mater. Today* **2007**, *10*, 28-33.

(5) Kippelen, B.; Brédas, J.-L., Organic Photovoltaics. *Energy Environ. Sci.* **2009**, *2*, 251-261.

(6) Zhang, L.; Colella, N. S.; Cherniawski, B. P.; Mannsfeld, S. C.; Briseno, A. L., Oligothiophene Semiconductors: Synthesis, Characterization, and Applications for Organic Devices. *ACS Appl. Mater. Interfaces* **2014**, *6*, 5327-5343.

(7) Grancini, G.; Santosh Kumar, R. S.; Abrusci, A.; Yip, H.-L.; Li, C.-Z.; Jen, A.-K. Y.; Lanzani, G.; Snaith, H. J., Boosting Infrared Light Harvesting by Molecular Functionalization of Metal Oxide/Polymer Interfaces in Efficient Hybrid Solar Cells. *Adv. Funct. Mater.* **2012**, *22*, 2160-2166.

(8) Ren, S.; Chang, L. Y.; Lim, S. K.; Zhao, J.; Smith, M.; Zhao, N.; Bulović, V.; Bawendi, M.; Gradečak, S., Inorganic–Organic Hybrid Solar Cell: Bridging Quantum Dots to Conjugated Polymer Nanowires. *Nano Lett.* **2011**, *11*, 3998-4002.

(9) Jiang, K.-J.; Manseki, K.; Yu, Y.-H.; Masaki, N.; Suzuki, K.; Song, Y.-l.; Yanagida, S., Photovoltaics Based on Hybridization of Effective Dye-Sensitized Titanium Oxide and Hole-Conductive Polymer P3HT. *Adv. Funct. Mater.* **2009**, *19*, 2481-2485.

(10) Zhu, R.; Jiang, C.-Y.; Liu, B.; Ramakrishna, S., Highly Efficient Nanoporous TiO2-Polythiophene Hybrid Solar Cells Based on Interfacial Modification Using a Metal-Free Organic Dye. *Adv. Mater.* **2009**, *21*, 994-1000.

(11) Coakley, K. M.; Liu, Y.; McGehee, M. D.; Frindell, K. L.; Stucky, G. D., Infiltrating Semiconducting Polymers into Self-Assembled Mesoporous Titania Films for Photovoltaic Applications. *Adv. Funct. Mater.* **2003**, *13*, 301-306.

(12) Abrusci, A.; Ding, I. K.; Al-Hashimi, M.; Segal-Peretz, T.; McGehee, M. D.; Heeney, M.; Frey, G. L.; Snaith, H. J., Facile Infiltration of Semiconducting Polymer into Mesoporous Electrodes for Hybrid Solar Cells. *Energy Environ. Sci.* **2011**, *4*, 3051-3058.

(13) Liu, J.; Tanaka, T.; Sivula, K.; Alivisatos, A. P.; Fréchet, J. M. J., Employing End-Functional Polythiophene to Control the Morphology of Nanocrystal-Polymer Composites in Hybrid Solar Cells. *J. Am. Chem. Soc.* **2004**, *126*, 6550-6551.

(14) Lin, Y.-Y.; Chu, T.-H.; Li, S.-S.; Chuang, C.-H.; Chang, C.-H.; Su, W.-F.; Chang, C.-P.; Chu, M.-W.; Chen, C.-W., Interfacial Nanostructuring on the Performance of Polymer/TiO2 Nanorod Bulk Heterojunction Solar Cells. *J. Am. Chem. Soc.* **2009**, *131*, 3644-3649.

(15) Liu, J.; Kadnikova, E. N.; Liu, Y.; McGehee, M. D.; Fréchet, J. M. J., Polythiophene Containing Thermally Removable Solubilizing Groups Enhances the Interface and the Performance of Polymer-Titania Hybrid Solar Cells. *J. Am. Chem. Soc.* **2004**, *126*, 9486-9487.

(16) Abrusci, A.; Santosh Kumar, R. S.; Al-Hashimi, M.; Heeney, M.; Petrozza, A.; Snaith, H. J., Influence of Ion Induced Local Coulomb Field and Polarity on Charge Generation and Efficiency in Poly(3-Hexylthiophene)-Based Solid-State Dye-Sensitized Solar Cells. *Adv. Funct. Mater.* **2011**, *21*, 2571-2579.

(17) Canesi, E. V.; Binda, M.; Abate, A.; Guarnera, S.; Moretti, L.; D'Innocenzo, V.; Sai Santosh Kumar, R.; Bertarelli, C.; Abrusci, A.; Snaith, H.; Calloni, A.; Brambilla, A.; Ciccacci, F.; Aghion, S.; Moia, F.; Ferragut, R.; Melis, C.; Malloci, G.; Mattoni, A.; Lanzani, G.; Petrozza, A., The Effect of Selective Interactions at the Interface of Polymer–Oxide Hybrid Solar Cells. *Energy Environ. Sci.* **2012**, *5*, 9068-9076.

(18) Boon, F.; Thomas, A.; Clavel, G.; Moerman, D.; De Winter, J.; Laurencin, D.; Coulembier, O.; Dubois, P.; Gerbaux, P.; Lazzaroni, R., Synthesis and Characterization of Carboxystyryl End-Functionalized Poly (3-hexylthiophene)/TiO2 Hybrids in View of Photovoltaic Applications. *Synth. Met.* **2012**, *162*, 1615-1622.

(19) Cossi, M.; Rega, N.; Scalmani, G.; Barone, V., Energies, Structures, and Electronic Properties of Molecules in Solution with the C-PCM Solvation Model. *J. Comput. Chem.* **2003**, *24*, 669-681.

(20) Frisch, M. J. *et al*. Gaussian 09, Revision B.01, *Gaussian Inc*. Wallingford CT, **2009**.

(21) Hanwell, M.; Curtis, D.; Lonie, D.; Vandermeersch, T.; Zurek, E.; Hutchison, G., Avogadro: an Advanced Semantic Chemical Editor, Visualization, and Analysis Platform. *J. Cheminf.* **2012**, *4*, 17.

(22) Abate, A.; Hollman, D. J.; Teuscher, J.; Pathak, S.; Avolio, R.; D'Errico, G.; Vitiello, G.; Fantacci, S.; Snaith, H. J., Protic Ionic Liquids as p-Dopant

for Organic Hole Transporting Materials and their Application in High Efficiency Hybrid Solar Cells. *J. Am. Chem. Soc.* **2013**, *135*, 13538-13548.

(23) Planells, M.; Abate, A.; Hollman, D. J.; Stranks, S. D.; Bharti, V.; Gaur, J.; Mohanty, D.; Chand, S.; Snaith, H. J.; Robertson, N., Diacetylene Bridged Triphenylamines as Hole Transport Materials for Solid State Dye Sensitized Solar Cells. *J. Mater. Chem. A* **2013**, *1*, 6949-6960.

(24) Snaith, H. J., How Should You Measure Your Excitonic Solar Cells? *Energy Environ. Sci.* **2012**, *5*, 6513-6520.

(25) Kanemitsu, Y.; Suzuki, K.; Tomiuchi, Y.; Shiraishi, Y.; Kuroda, M.; Nabeta, O., Luminescence from Oligothiophenes and Thiophene-Based Oligomers. *Synth. Met.* **1995**, *71*, 2209-2210.

(26) Inamdar, S. N.; Ingole, P. P.; Haram, S. K., Determination of Band Structure Parameters and the Quasi-Particle Gap of CdSe Quantum Dots by Cyclic Voltammetry. *ChemPhysChem* **2008**, *9*, 2574-2579.

(27) Knupfer, M., Exciton Binding Energies in Organic Semiconductors. *Appl. Phys. A* **2003**, *77*, 623-626.

(28) Jones, B. A.; Facchetti, A.; Wasielewski, M. R.; Marks, T. J., Tuning Orbital Energetics in Arylene Diimide Semiconductors. Materials Design for Ambient Stability of n-Type Charge Transport. *J. Am. Chem. Soc.* **2007**, *129*, 15259-15278.

(29) Cappel, U. B.; Plogmaker, S.; Johansson, E. M.; Hagfeldt, A.; Boschloo, G.; Rensmo, H., Energy Alignment and Surface Dipoles of Rylene Dyes Adsorbed to TiO2 Nanoparticles. *Phys. Chem. Chem. Phys.* **2011**, *13*, 14767-14774.